# Intramolecular Electron Transfer: Independent (Ground State) Adiabatic (Chemical) and Nonadiabatic Reaction Pathways in Bis(hydrazine) Radical Cations

**Eva Fernández,[†] Lluís Blancafort,*[,†] Massimo Olivucci,*[,‡] and Michael A. Robb*[,†]**

*Contribution from the Department of Chemistry, King's College London, Strand, London WC2R 2LS, UK, and Istituto di Chimica Organica, Università degli Studi di Siena, Via Aldo Moro, I-53100 Siena, Italy*

*Received January 3, 2000. Revised Manuscript Received April 11, 2000*

**Abstract:** Two different mechanistic processes in intramolecular electron transfer chemistry have been studied with the complete active space self-consistent field quantum chemical method for a model bis(hydrazine) radical cation. These correspond to (a) a chemical electron transfer, where a reaction intermediate or a transition structure exist with the charge localized on the linker, and (b) a nonadiabatic electron transfer, where the bridge remains neutral. These processes coexist on the same potential energy surface. They are characterized by very different reaction coordinates and are thus distinct elements of the mechanistic spectrum of intramolecular electron transfer in organic radical cations. The energetically favored chemical electron-transfer process involves conventional reaction paths. In contrast, the nonadiabatic electron-transfer process involves an unconventional reaction path, which connects reactant and products via an un-avoided (i.e., real) crossing seam (i.e. an $(n-1)$-dimensional intersection, where $n$ is the number of vibrational degrees of freedom of the system) between two different adiabatic potential energy surfaces. Our results, computed for a model compound, differ from Nelsen's experimental results, and thus demonstrate the importance of the hydrazine substituents and the aromatic spacer.

## Introduction

Using modern computational chemistry methods, the molecular structure change occurring during a chemical transformation, i.e., the reaction coordinate, can be determined in a fully unbiased way. A reaction coordinate is defined as the coordinate corresponding to the minimum energy path connecting the reactant and the product structures within the complete set of the internal molecular coordinates (which correspond to the $n$ vibrational degrees of freedom of the reacting system). Gradient-based computational methods can be used routinely to compute such paths. However, the power of modern computations contrasts with the apparent simplicity of the traditional qualitative models used for rationalizing chemical processes. State-crossing models such as those of Bell−Evans−Polany, Hammond, Woodward−Hoffmann,[1] and Marcus[2] tend to convey an oversimplified monodimensional view of the reaction coordinate which is, in reality, a highly complex interplay of several internal coordinates of the molecule. These models also ignore the "mechanistic spectrum" of a chemical reaction: different, higher energy paths may exist along very different reaction coordinates. A mechanistic knowledge which includes several possible pathways can play a role in rationalizing or predicting the sensitivity of the reaction to substituents and environment.

While in the past the rigorous determination of the "mechanistic spectrum" of different covalent and ionic organic reactions has been tackled via reaction-path calculations (e.g., in pericyclic reactions, synchronous and asynchronous diradical pathways have been studied), similar studies of electron-transfer processes are rare.[3] In this paper, intramolecular electron transfer (IET) in bis(hydrazine) radical cations,[4] with two hydrazine units coupled by an aromatic linker, has been studied with ab initio complete active space (CASSCF) calculations. For the model compound **1** (Scheme 1), we have located the reaction coordinates that describe two different IET mechanisms. These correspond to a substantially concerted "nonadiabatic" mechanism (NAET) and to a stepwise "chemical" (chemical electron transfer, CET) mechanism.

The analysis of our computed data reveals that both mechanisms can be considered to be limiting cases of a Marcus−Hush (MH) model that includes three diabatic states: the two charge-localized states $U_{loc}$ and $U_{loc'}$ and a third state with the charge located on the bridge $U_{br}$. In the usual superexchange mechanism (Figure 1b), the two localized states are indirectly coupled via the bridge state. The effective coupling matrix element $V_{eff}$ in Marcus−Hush theory[2] arises by indirect interaction (usually called through-bond) between $U_{loc}$ and $U_{loc'}$ through the bridge diabatic potential curve $U_{br}$. In our nonadiabatic reaction coordinate (see Figure 1a), the interaction of the bridge state with the charge localized states is almost negligible due to a high energy $U_{br}$ and to a poor orbital overlap of the bridge with the hydrazine units. In this extreme case, the coupling element $V_{eff}$ between the diabatic states (Figure 1a) is virtually zero, and the crossing between the ground and excited-state

[†] King's College London.
[‡] University of Siena.

(1) Salem, L. In *Electrons in Chemical Reactions: First Principles*; John Wiley & Sons: New York, 1982.

(2) (a) Newton, M. D. *Chem. Rev.* **1991**, *91*, 767−792. (b) Sutin, N. *Prog. Inorg. Chem.* **1983**, *30*, 441−498. (c) Marcus, R. A. *Annu. Rev. Phys. Chem.* **1964**, *15*, 155−196.

(3) (a) Reddy, A. C.; Danovich, D.; Ioffe, A.; Shaik, S. *J. Chem. Soc., Perkin Trans. 2* **1995**, 1525−1539. (b) Sastry, G. N.; Shaik, S. *J. Am. Chem. Soc.* **1998**, *120*, 2131−2145.

(4) (a) Nelsen, S. F.; Ismagilov, R. F.; Powell, D. R. *J. Am. Chem. Soc.* **1996**, *118*, 6313−6314. (b) Nelsen, S. F.; Ismagilov, R. F.; Powell, D. R. *J. Am. Chem. Soc.* **1997**, *119*, 10213−10222. (c) Nelsen, S. F.; Ismagilov, R. F.; Powell, D. R. *J. Am. Chem. Soc.* **1998**, *120*, 1924−1925.

10.1021/ja000013c CCC: $19.00 
Published on Web 07/21/2000

**Scheme 1**

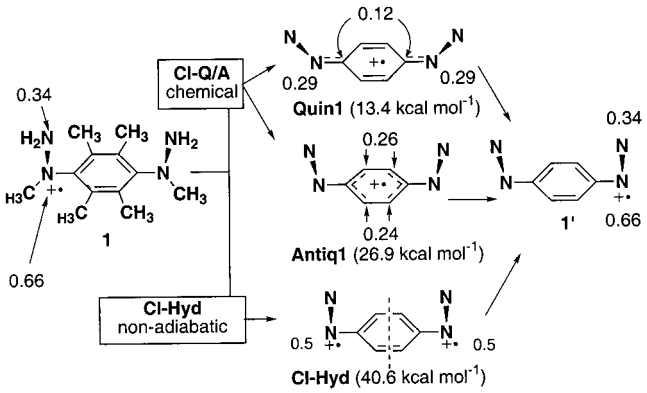


potential energy surfaces is in fact unavoided. This situation leads to nonadiabatic chemistry (i.e., passage from reactant to product through the TS region that requires vibronic coupling between the two crossing states). In contrast, in the chemical mechanism (see Figure 1c),[5] $U_{br}$ is stable and the orbital overlap effective, so that the interaction between the bridge state and the two localized states is large, giving rise to a triple-well ground state adiabatic potential energy (Figure 1c). In the region of the central well, the charge is partly localized on the benzene linker as the bridge state dominates the wave function.

In summary, while the CET process for our model compound **1** is adiabatic, and involves the formation of a short-lived intermediate or the passage through a flat transition state (**Quin1** and **Antiq1** in Scheme 1, respectively), the alternative process must be nonadiabatic. However, both processes are part of the same IET mechanistic spectrum as they coexist on the same *n*-dimensional ground-state adiabatic energy surface along very different reaction coordinates.

In recent work, we and others have shown that real crossings between adiabatic potential energy surfaces of the same spin multiplicity, such as conical intersections (CI), can be used to rationalize the existence of different (potentially competitive) reaction paths of organic radical cations.[6,7] For example, the reactivity of the cyclopentane-1,3-diyl radical cation is determined by intermediates and transition states that lie in the "moat" of a CI[6,8] (notice that these surface crossings are "real" intersections of adiabatic states, within the Born−Oppenheimer approximation, and not the result of a mathematical model involving diabatic states). Thus, the topology of the mechanistically relevant part of the potential energy surface of this species can be understood by mapping the surface along two characteristic directions departing from the CI. These are the gradient difference (GD) and derivative coupling (DC) coordinates (vectors), which are obtained by calculation. The various, rigorously computed (i.e., fully unconstrained geometry optimization is used in all cases) minima and transition structures can then be topologically related to the conical intersections within the plane of the GD and DC coordinates. The information is pieced together in two-dimensional "cartoons" which provide a "global" view of the mechanistic spectrum of the species under investigation. In our present quantum chemical study of the bis(hydrazine) radical cation model **1**, we have used this computational strategy to investigate the different IET reaction coordinates. The resulting energy surface pictures illustrate the mechanistically relevant part of the ground-state potential surface and reveal the structure of the region where the computed IET paths are located.

The energy surface associated with the CET mechanisms is given in Figure 2a. It is apparent that CET occurs along two reaction paths located in the "moat" surrounding a point of conical intersection. The CI (**CI-Q/A** in Figure 2a) occurs between the quinoid and antiquinoid diabatic states where the charge is localized in the benzene bridge (Figure 2c). The space of geometric coordinates which contain the moat ($\mathbf{X_1}$ and $\mathbf{X_2}$ in Figure 2a) corresponds approximately to the GD and DC vectors (see the Computational Details section for a definition of the DC and GD vectors). The DC vector $\mathbf{X_2}$ in Figure 2a is the "ideal" electron-transfer coordinate since it describes the coordinate along which the mixing of the electronic wave functions (the initial electronic configuration and the final one) takes place. The degenerate charge-localized reactant and product structures **1** and **1′** are connected via two reaction paths ($\mathbf{Q_1}$ and $\mathbf{Q_2}$ in Figure 2). $\mathbf{Q_1}$ is stepwise and passes through a quinoid intermediate $\mathbf{Quin_1}$ (a local energy minimum) with the charge partially localized on the benzene linker. $\mathbf{Q_2}$ is a concerted path passing through the transition state structure $\mathbf{Antiq_1}$ (a local energy saddle point), which has a charge distribution different from $\mathbf{Quin_1}$. $\mathbf{Q_1}$ and $\mathbf{Q_2}$ may be associated with the MH diagram type of Figure 1c. In conclusion, the CET potential energy surface structure is very similar to that of the previously reported housane radical cation rearrangement.[6,8] In that surface the unpaired electron of a planar, charge-localized radical cation structure is formally transferred across a five-membered carbon ring involving passage through charge-delocalized configurations.

In contrast with the CET process, the adiabatic potential energy surface associated with the alternative process shows an unconventional structure (Figure 3a) where a nonavoided crossing (**CI-Hyd**) is substantially coincident with the "transition state" of the IET path. This is consistent with the model of Figure 1a. The crossing occurs between the two hydrazine-localized states. The existence of a ground-state reaction coordinate (i.e., the minimum energy path $\mathbf{Q_3}$ of Figure 3a) passing through a nonavoided crossing of two adiabatic potential energy surfaces has never been reported before. Indeed, such a situation seems highly improbable since nonavoided crossings between energy surfaces of the same spin multiplicity (in our case two doublet states) correspond, in general, to CI points. Ground-state minimum energy paths are usually located far from such crossing points in virtue of the conical shape of the energy surface surrounding the CI, as clearly illustrated by the CET energy surface of Figure 2a. Very remarkably our calculations show that **CI-Hyd** is a point belonging to an $(n - 1)$-dimensional region (a hyperplane) of the potential energy surface where the energy separation of the ground and excited states is less than a few kilocalories per mole. This "U" shaped region (represented as a bold line in Figure 3a) forms, effectively, a seam of nonavoided crossing points which acts as a sharp "mountain pass" between the reactant and product valleys. Thus, the separation between the two near-degenerate surfaces at **CI-Hyd** is very small (see Figure 3b) and the reaction must therefore lie at the limit between the adiabatic and the nona-

(5) (a) See ref 3 in ref 4c. (b) We use the term "chemical mechanism" because the potential energy surface of the bridge ($U_{br}$) lies below that of the charge-localized states ($U_{loc}$) in the transition-state region (Figure 1c). Alternatively, we use the term superexchange mechanism when $U_{br}$ lies above $U_{loc}$ (Figure 1b). See: Cannon, R. D. In *Electron-Transfer Reactions*; Butterworth: London, 1980; pp 223−237.

(6) Blancafort, L.; Adam, W.; González, D.; Olivucci, M.; Vreven, T.; Robb, M. A. *J. Am. Chem. Soc.* **1999**, *121*, 10583−10590.

(7) Sastry, G. N.; Bally, T.; Hrouda, V.; Cársky, P. *J. Am. Chem. Soc.* **1998**, *120*, 9323−9334.

(8) (a) Bernardi, F.; Olivucci, M.; Robb, M. A. *Chem. Soc. Rev.* **1996**, *25*, 321−328. (b) Klessinger, M.; Michl, J. *Excited States and Photochemistry of Organic Molecules*; VCH: New York, 1995; pp 183−184. (c) Davidson, E. R. *J. Am. Chem. Soc.* **1977**, *99*, 397−402.

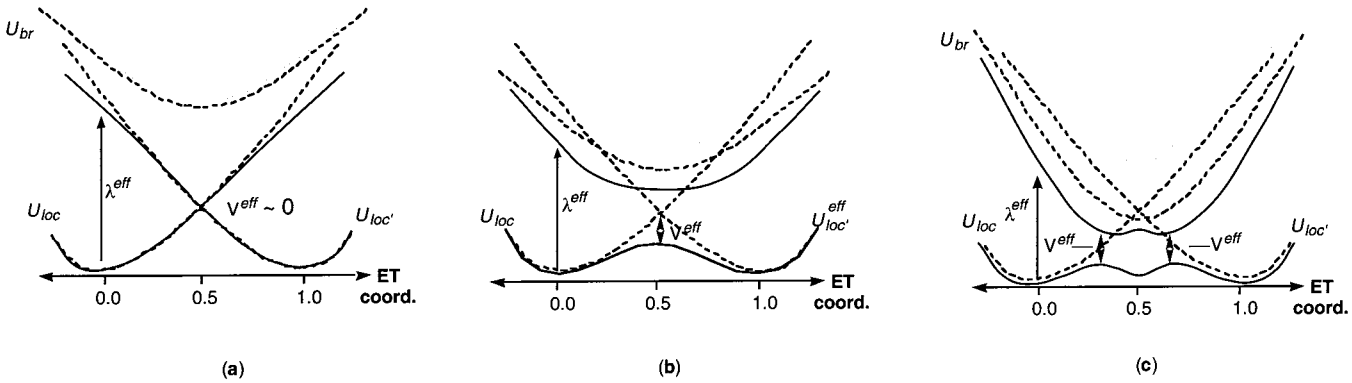


**Figure 1.** General plot of the parabolic diabatic surfaces (charge-localized states $U_{loc}$ and $U_{loc'}$ and bridge-localized $U_{br}$; broken lines) and adiabatic surfaces (full lines) for IET on compound **1** ($\Delta G = 0$). A third, higher energy adiabatic surface is shown in gray. Direct interaction between $U_{loc}$ and $U_{loc'}$ is neglected. (a) Marcus−Hush plot for a high-energy bridged state (or noninteracting bridged state) leading to a "nonadiabatic" mechanism (NAET). (b) Marcus−Hush plot for a lower energy bridged state leading to indirect $U_{eff}$ and $U_{eff'}$ interaction (super-exchange). (c) Marcus−Hush type plot for a very stable $U_{br}$ potential leading to a CET mechanism. $\lambda$ is the optical excitation and $V$ the coupling matrix element.

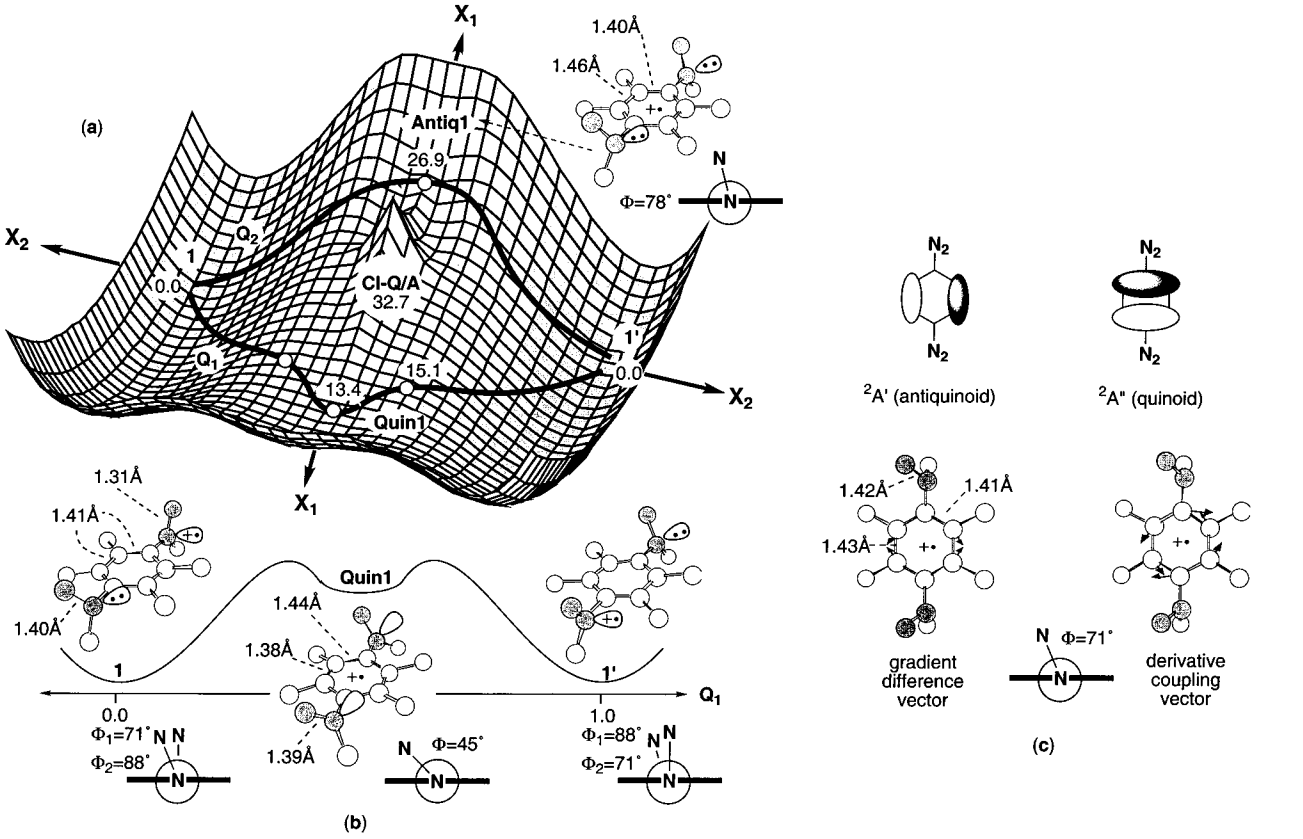


**Figure 2.** Schematic representation of the potential energy surface around **CI-Q/A** (CET). (a) Potential energy surface topology around **CI-Q/A** along $\mathbf{X_1}$ (gradient difference and hydrazine rotation, $||X_1|| \neq 0$) and $\mathbf{X_2}$ (derivative coupling and hydrazine rotation), including the two adiabatic IET pathways $\mathbf{Q_1}$ and $\mathbf{Q_2}$ that avoid the crossing surrounding the cone. (b) Cut through the lowest energy path $\mathbf{Q_1}$ showing the geometrical changes (ball-and-stick structures and Newman projections) along the reaction coordinate. (c) Singly occupied orbitals for the crossing states at **CI-Q/A** and gradient difference and derivative coupling vectors.

diabatic regime.[9] The corresponding DC vector describes both the electron-transfer coordinate and the nonadiabatic process which are dominated by the extremely rapid change of the wave function from that of the charge localized state of **1** to that of **1′** (i.e. from the $U_{loc}$ to $U_{loc'}$ diabatic states).

In conclusion, our computational results can be related to MH theory, by which IET processes are usually analyzed.[2] The CET mechanism can be simply understood in terms of two weakly interacting diabatic states (with the charge localized on the hydrazine units) which interact with a bridge state (with the charge localized on the bridge). In contrast, the NAET mechanism originates from the first two weakly interacting states only, as the third diabatic state does not interact. As we shall discuss below, the reason for the coexistence of the two mechanisms in the bis(hydrazine) radical cation model can be primarily understood in terms of the very different nature of the corresponding reaction coordinates.

## Computational Details

All calculations (CASSCF(9,8)/6-31g* geometry optimizations) were carried out with Gaussian 98, Revision B.[10] See Table 1 for energetics. Preliminary calculations suggested that **1** was the simplest model to

(9) Farazdel, A.; Dupuis, M.; Clementi, E.; Aviram, A. *J. Am. Chem. Soc.* **1990**, *112*, 4206.

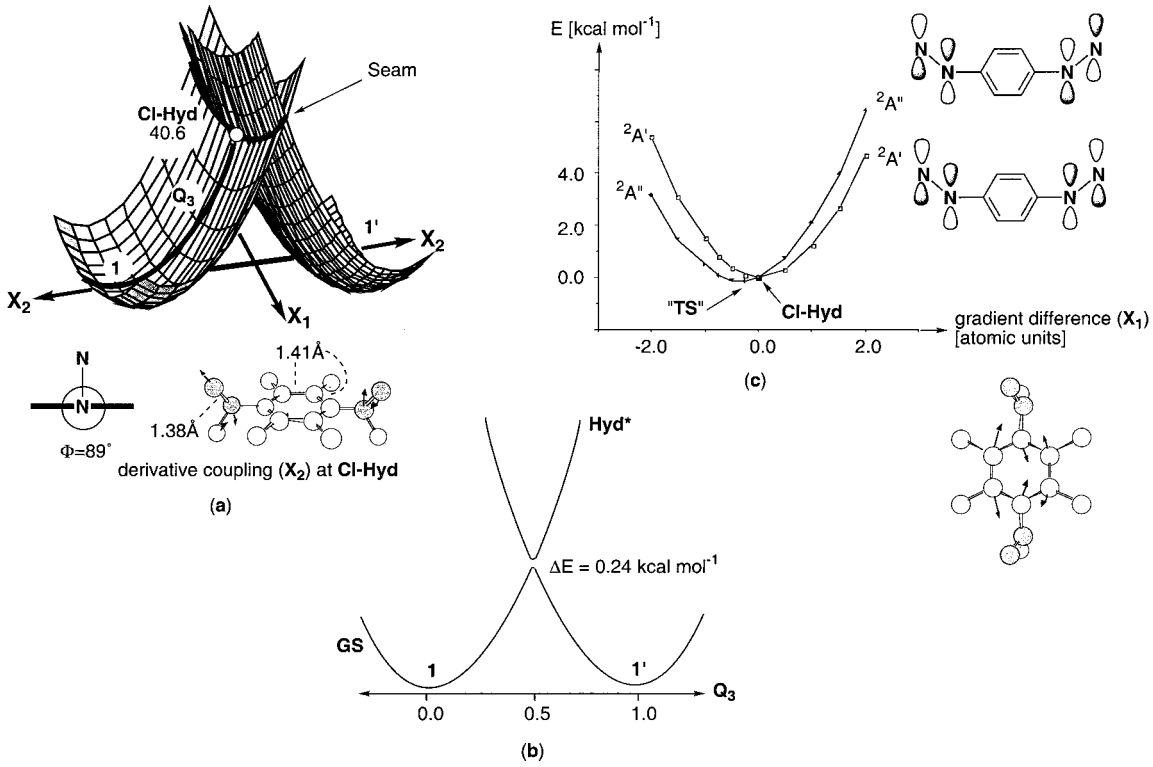


**Figure 3.** Schematic representation of the potential energy surface around **CI-Hyd**. (a) Potential energy surface topology around **CI-Hyd** along $\mathbf{X_1}$ (gradient difference, $||X_1|| = 0$) and $\mathbf{X_2}$ (derivative coupling and hydrazine rotation). (b) Cut through the nonadiabatic coordinate $\mathbf{Q_3}$. (c) Singly occupied orbitals for the crossing states at **CI-Hyd** and linear coordinate calculated along the gradient difference $\mathbf{X_1}$.

**Table 1.** CASSCF(9,8)/6-31G* Optimized Energies

| structure | symmetry | state | energy (au) | $E_{rel}$ (kcal mol$^{-1}$) |
|---|---|---|---|---|
| **1** | $C_1$ | 2A | −684.7713 | 0.0 |
| **CI-Q/A** | $C_s$ | 2A′/2A″ | −684.7193 | 32.7 |
| **Quin$_1$** | $C_s$ | 2A″ | −684.7500 | 13.4 |
| **Antiq$_1$** | $C_s$ | 2A′ | −684.7284 | 26.9 |
| **CI-Hyd** | $C_s$ | 2A′/2A″ | −684.7066 | 40.6 |

avoid a preference for charge-delocalized structures where the hydrazine units are coplanar with the aromatic ring. The "ideal" active space for our calculations would consist of the six benzene $\pi$ orbitals and the four nitrogen lone pairs. Two of the orbitals (the bonding combinations of neighboring nitrogen orbitals) had an occupation close to 2.00 in our calculations, and the active space was reduced to 9 electrons in 8 orbitals.

For the analytical frequency calculations at **Quin$_1$** and **Antiq$_1$**, the active space was reduced to (7,7) and (5,6), respectively, by eliminating the orbitals which had occupation >1.98. The energies for the IET coordinate $\mathbf{Q_1}$ through **Quin$_1$** were calculated with a linearly interpolated reaction coordinate between the localized minimum **1** and **Quin$_1$** (see Figure S1, Supporting Information). The "charges" indicated in Scheme 1 are an indication of the distribution of the charge in the active space. They are obtained by subtracting the occupation numbers (diagonal elements of the one-electron density matrix) of the localized active orbitals (computed with the full active space of 13 orbitals) from the "full" occupation, 1.0 for carbon and 2.0 for nitrogen atoms.

The PES presented in Figures 2 and 3 are "cartoons" intended to illustrate the topological relationship between the optimized structures (state crossings and minima) and the two directions gradient difference (GD) $\langle\partial(E_1 - E_2)/\partial Q\rangle$, and derivative coupling (DC) $\langle\Psi|(\partial H/\partial Q)\Psi\rangle$ (which is parallel to the nonadiabatic coupling $\langle\Psi_1(\partial\Psi_2/\partial Q)\rangle$), a vector which describes the geometrical deformation that yields the fastest change in electronic structure. In the case of IET, this vector corresponds to the electron-transfer coordinate, which lifts the degeneracy at the conical intersection.[8] The quantities are computed (like a gradient) during the conical intersection optimization. As the coordinates for our schematic representation of the potential surface topology, in Figures 2a and 3a we use the vectors $\mathbf{X_1}$ and $\mathbf{X_2}$. These are coincident with GD and DC, respectively, in the vicinity of the CI. However, as one moves away from the CI, other geometric coordinates mix with $\mathbf{X_1}$ and $\mathbf{X_2}$ along the reaction path. In our case, $\mathbf{X_1}$ and $\mathbf{X_2}$ mix with the rotation of the hydrazines (except in the case of **CI-Hyd**, where $\mathbf{X_1}$ is given purely by the GD vector since the delocalized symmetry-constrained minima are extremely close to the CI, see also Figure 3c). The complete reaction pathways for IET are tangent to the plane of $\mathbf{X_1}$ and $\mathbf{X_2}$ at the conical intersection. Initial displacement along the symmetry-breaking coordinate $\mathbf{X_2}$ (related to DC) in both directions ultimately leads to the localized minima **1** and **1′**, while initial displacement along the totally symmetric coordinate $\mathbf{X_1}$ (related to GD) leads ultimately to the delocalized, symmetry-constrained minima that are the intermediates or TS's for the IET. Accordingly, the IET coordinates $\mathbf{Q_1}$−$\mathbf{Q_3}$ are qualitatively defined as the reaction paths that connect **1** and **1′** through three different transition-state regions.

## Results and Discussion

We have optimized the structure of the radical cation of the meso diastereomer of **1** which has a plane of symmetry (mirroring the two hydrazines) in its neutral form. As shown in Scheme 1 the plane of symmetry is lost at the resulting equilibrium geometry (structure **1** in Figure 2b). The optimized bond lengths are 1.40 Å for the nitrogen−nitrogen bond at the neutral hydrazine and 1.31 Å at the charged one. These values agree well with the crystallographic data for the synthesized analogues.[4] However, the dihedral angles $\Phi$ between the phenyl-substituted nitrogen lone pair and the $\pi$ orbitals of the benzene ring differ from the synthesized analogues because of the

(10) Frisch, M. J.; Trucks, G. W.; Schlegel, H. B.; Gill, P. M. W.; Johnson, B. G.; Robb, M. A.; Cheeseman, J. R.; Keith, T.; Petersson, G. A.; Montgomery, J. A.; Raghavachari, K.; Al-Laham, M. A.; Zakrzewski, V. G.; Ortiz, J. V.; Foresman, J. B.; Cioslowski, J.; Stefanov, B. B.; Nanayakkara, A.; Challacombe, M.; Peng, C. Y.; Ayala, P. Y.; Chen, W.; Wong, M. W.; Andres, J. L.; Replogle, E. S.; Gomperts, R.; Martin, R. L.; Fox, D. J.; Binkley, J. S.; Defrees, D. J.; Baker, J.; Stewart, J. P.; Head-Gordon, M.; Gonzalez, C.; Pople, J. A. Gaussian, Inc.: Pittsburgh, PA, 1999.

different substitution pattern of our model **1** (see Figure 2b). In **1**, the charge-bearing hydrazine is perpendicular to the aromatic ring, and $\Phi$ is approximately 90° for the charged unit (70° for the neutral hydrazine). In Nelsen's compounds, $\Phi$ is 30−50° for the neutral hydrazines and 50−70° for the charged units.[4a,b]

The CET mechanism (of lowest energy) occurs along two different paths located in the vicinity of a CI of $C_s$ symmetry (**CI-Q/A** in Scheme 1 and Figure 2a), where the charge is localized on the benzene ring. **CI-Q/A** lies at 32.7 kcal mol$^{-1}$ relative to **1** and is the intersection of the benzene-like quinoid $^2$A″ and antiquinoid $^2$A′ states (Figure 2c). The GD and DC coordinates (Figure 2c) are analogous to the corresponding coordinates for the Jahn−Teller CI of $D_{6h}$ symmetry in benzene radical cation.[11] Displacement along $\mathbf{X_2}$ (a combination of the DC coordinate and rotation of the hydrazines) in the two opposite directions leads to the minima **1** and **1′**, respectively. Displacement from **CI-Q/A** along $\mathbf{X_1}$ (a combination of the orthogonal GD coordinate shown in Figure 2c and rotation of the hydrazines) leads to a quinoid structure $\mathbf{Quin_1}$ (13.4 kcal mol$^{-1}$ above **1**) and the antiquinoid structure $\mathbf{Antiq_1}$ (26.9 kcal mol$^{-1}$ above **1**) in opposite directions. Analytical frequency calculations show that $\mathbf{Quin_1}$ and $\mathbf{Antiq_1}$ are an intermediate (a local minimum) and a TS of $C_s$ symmetry. These structures define a stepwise and a concerted CET path (chemical, since the charge is localized in the bridge).[5b] Thus the corresponding IET paths $\mathbf{Q_1}$ and $\mathbf{Q_2}$ are located on the moat that surrounds **CI-Q/A**. The intermediate $\mathbf{Quin_1}$ is a shallow minimum along the lowest energy IET path $\mathbf{Q_1}$ (see also Supporting Information). At $\mathbf{Quin_1}$, the hydrazine lone pairs get aligned with the benzene $\pi$ orbitals by hydrazine rotation, and the angle $\Phi$ is reduced to approximately 45° for both hydrazines (Figure 2b). Orbital overlap is essential in this mechanism, as the charge is partly delocalized into the benzene ring (see the "charges" in Scheme 1). At $\mathbf{Antiq_1}$, the charged hydrazine group of **1** rotates in the opposite direction to $\mathbf{Quin_1}$. This puts the hydrazine units almost perpendicular to the ring ($\Phi = 78°$), as the charge gets localized in the spacer.

The nonadiabatic electron-transfer mechanism is characterized by a reaction path passing through the minimum energy point of an approximate seam of crossing between the $^2$A′ and $^2$A″ hydrazine-localized states (the semioccupied orbitals for both states are shown in Figure 3c). This minimum corresponds to the optimized **CI-Hyd** structure. At **CI-Hyd**, the hydrazine units are perpendicular to the benzene ring ($\Phi = 89°$, Figure 3b), and the relative energy is 40.6 kcal mol$^{-1}$. The DC coordinate (Figure 3a) is the antisymmetric stretching of the two nitrogen−nitrogen bonds (which are equivalent at **CI-Hyd**) and leads to the localized minima **1** and **1′**. The electron-transfer path $\mathbf{Q_3}$ (tangent to $\mathbf{X_2}$ at **CI-Hyd**) corresponds to a rotation of the hydrazine angles together with the antisymmetric stretching of the nitrogen−nitrogen bonds, while the spacer remains neutral (see the "charges" in Scheme 1). The magnitude of the orthogonal totally symmetric GD vector ($\mathbf{X_1}$) is small (0.018 au compared to 0.083 au for the derivative coupling vector). Further, the magnitude of the gradients of the states that cross is very small (0.018 and 0.002 au). The symmetry-constrained energy minima located along $\mathbf{X_1}$ (i.e., the analogues of the $\mathbf{Quin_1}$ and $\mathbf{Antiq_1}$ of the CET mechanism) that correspond to the states crossing at **CI-Hyd** could not be optimized because of their closeness to the CI. Thus, to characterize the crossing, we calculated a series of single points obtained following the gradient difference coordinate in both directions from **CI-Hyd**. The resulting linear coordinate (Figure 3c) shows that the splitting between the $^2$A′ and $^2$A″ surfaces along the gradient difference coordinate is very limited, indicating that **CI-Hyd** is (approximately) a crossing seam rather than a conical intersection. The calculated energy profile along the $\mathbf{X_1}$ coordinate confirms that the energy minimum of this coordinate (marked "**TS**" in Figure 3c) is almost coincident with **CI-Hyd**, and the separation between the states (Figure 3b) is ca. 0.24 kcal mol$^{-1}$ (0.01 eV). The limit for adiabatic regime for ET is given by $V_{el} = k_BT = 0.025$ eV at 298 K.[9] Thus, our approximate calculations (the point "**TS**" was not optimized) indicate that the mechanism through **CI-Hyd** will be nearly nonadiabatic.

**Table 2.** CASSCF(9,8)/6-31g* Excitation Energies at the Localized Minimum **1** (calculated with state average over the three states) and the Model Structure **2**

| compd | state | energy (au) | $E_{rel}$ (kcal mol$^{-1}$) |
|---|---|---|---|
| **1** | $D_0$ (hydrazine-localized) | −684.7301 | 0.0 |
| | $D_1$ (quinoid) | −684.6635 | 41.8 |
| | $D_2$ (antiquinoid) | −684.6621 | 42.7 |
| **2** | $D_0$ (hydrazine-localized) | −528.6012 | 0.0 |
| | $D_1$ (hydrazine-localized) | −528.5299 | 44.7 |

In summary, the potential energy surface in the region of **CI-Hyd** is effectively a crossing "seam" (shown as a bold line in Figure 3a). This entity can be seen as a special case of a conical intersection where the GD vector (related to $\mathbf{X_1}$) is of zero length while the DC vector (related to $\mathbf{X_2}$) retains its interpretation as the electron-transfer coordinate.[12] Thus, the degeneracy occurs in $n - 1$ coordinates rather than $n - 2$, and the situation is similar to that of a singlet−triplet crossing. (In fact in a singlet−triplet crossing one of the two vectors, in this case DC, vanishes identically due to the different spin multiplicity of the intersecting states while the other, the GD vector, has a finite length.) Notice that the physical basis for the occurrence of a crossing seam rather than a conical intersection lies in the large separation between the hydrazine units ($r_{N,N} = 5.6$ Å for the phenyl-substituted nitrogens) and in the poor overlap between the hydrazine lone pairs and the orbitals of the linker (angle $\Phi = 89°$). Thus, the seam found in our model is an extreme case of the MH mechanism where the coupling between the states is close to zero (see Figure 1a). Moreover, our calculations, where **CI-Hyd** was optimized without artificial constraints, do show that on the ground-state potential energy surface of **1** two independent mechanisms coexist through different reaction coordinates, i.e., along different regions of the surface.

In the MH analysis, the charge-transfer band ($\lambda$ in Figure 1) is used to obtain the model parametrization. The lowest energy excited state calculated at the localized minimum **1** involves charge transfer (CT) between the bridge and the charged hydrazine unit (see Table 2), and the calculated CASSCF(9,8)/6-31G* energy was 42 kcal mol$^{-1}$ (684 nm) for the lowest absorption. Nelsen's anthracenyl-linked hydrazine[4c] resembles our model **1** in that the lowest optical band is a CT from the

(11) Blancafort, L.; Fernández, E.; Robb, M. A. Unpublished results. See also: (a) Lunell, S.; Gauld, J. W.; Kadam, R. M.; Itagaki, Y.; Lund, A. *Adv. Quantum Chem.* **1999**, *35*, 339−355. (b) Huang, M.-B.; Lunell, S. *J. Chem. Phys.* **1990**, *92*, 6081−6083.

(12) There is an apparent contradiction between our calculation and Figure 3b, where the gradients of the crossing states are effectively zero at **CI-Hyd**, and Figure 3a, where the two surfaces appear to have large different gradients. This is due to the fact that, at **CI-Hyd** ($C_s$ symmetry), the crossing states have A″ and A′ symmetry (shown in Figure 3c) and the charge is delocalized. At this point the gradient difference is totally symmetric ($\mathbf{X_1}$), while the derivative coupling is not totally symmetric ($\mathbf{X_2}$). As one moves away from the crossing, the adiabatic states become the charge localized ones, so the coordinate $\mathbf{X_2}$ becomes the gradient difference and the coordinate $\mathbf{X_1}$ becomes the derivative coupling. This problem is discussed in a more detailed way in the following: Atchity, G. J.; Xantheas, S. S.; Ruedenberg, K. *J. Chem. Phys.* **1991**, *95*, 1862.

aromatic spacer to the hydrazine. However, it would not be correct to describe the IET from **1** to $\mathbf{Quin_1}$ with MH theory. In fact, this theory assumes that there is a weak direct orbital overlap between the charge-bearing units,[2c] and our calculations show that there is a significant overlap between the hydrazine and benzene orbitals at $\mathbf{Quin_1}$. In addition, the three-state MH type model, proposed by Nelsen and co-worker's for the analysis of the anthracenyl-linked bis(hydrazine),[4c] must be applied with caution. *In this model, the coordinates for the different processes (CET and nonadiabatic) are assumed to be the same, while our calculations demonstrate that different (not necessarily competitive) IET paths may coexist on the same potential energy surface along different reaction coordinates.*

For Nelsen's example with a tetramethyl-substituted phenyl spacer, the lowest observed optical band is CT between the hydrazines[4a,b] corresponding to a superexchange mechanism. In our computations the lowest excited state involves charge transfer between the bridge and the charged hydrazine unit. The origin of the difference lies in the dihedral angles between the benzene and hydrazines in our structure and Nelsen's compounds. The vertical excitation energy was computed for a model compound **2** which has exactly the same geometry

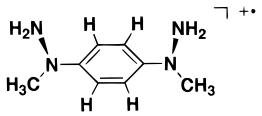


Structure **2**

(including the dihedral angles Φ and the bond lengths at the hydrazines) as Nelsen's reported bis(hydrazine) with the tetramethyl-substituted phenyl spacer (see Table 2).[4b] The only difference is that all alkyl substituents (with the exception of a methyl group on each of the nitrogens α to the ring) have been removed. Our calculations show that the change in the orientation of the hydrazines with respect to the ring leads to a change in the lowest excitation, which has mainly hydrazine−hydrazine character (with some quinoid character) in **2** (calculated energy 44.7 kcal $mol^{-1}$, 639 nm).

Nelsen has reported single-step IET with much smaller barriers (2.7−4.8 kcal $mol^{-1}$).[1] The higher degree of substitution of Nelsen's compounds is the major effect that makes them conformationally more rigid and implies that the geometric changes accompanying the IET are smaller than those in our model, which is reflected in smaller barriers. Also, in Nelsen's compounds[4] the steric constraint implies that the angles Φ, which in turn determine the magnitude of the coupling, differ from 90° at the TS region. Therefore, in these cases the superexchange mechanism will apply rather than the nonadiabatic and chemical ones, as for our model **1**. IET in Nelsen's compounds may be well described by MH theory. Nelsen's compounds are very rigid. Thus, there will only be very small geometric changes along the IET coordinate **Q**. Accordingly, the assumption of the MH analysis, that the coupling element $V$ is independent of **Q**, may be a good approximation.[2] However, in our model **1**, this assumption is not valid.

## Conclusions

Two possible mechanisms (CET and nonadiabatic) for IET are associated with different regions of the potential energy surface and are centered around distinct adiabatic potential energy surface intersections (a CI and an approximate seam of crossing). The intersections obtained from our CASSCF calculations are physical (i.e., nonavoided) within the Born−Oppenheimer approximation and not the result of a mathematical model involving the crossing of diabatic states. For CET there are *two* possible distinctive adiabatic paths (viz., $\mathbf{Q_1}$ and $\mathbf{Q_2}$ in Figure 2a). In contrast, in the case of NAET, there is a single path ($\mathbf{Q_3}$ in Figure 3) defined by the lowest energy point along a crossing seam (Figure 3a) that "operates" like a nonadiabatic transition state. In the lowest energy chemical mechanism, the transition state region associated with $\mathbf{Quin_1}$ is much lower in energy than the TS region for the nonadiabatic case, so that, for our model compound, we predict a chemical mechanism via a stepwise path. Of course changes in the nature of the linker, donor/acceptor, or type and degree of substitution may result in a preference for a different path.

Analysis of the $\mathbf{Q_1}$, $\mathbf{Q_2}$, and $\mathbf{Q_3}$ paths demonstrates that the CET and NAET processes occur along distinct reaction coordinates made of rotation of the hydrazine angles together with the antisymmetric stretching of the nitrogen−nitrogen bond. In the CET, the nitrogen lone pairs are aligned with the aromatic $\pi$ system, and the charge delocalizes into the bridge. However, in the nonadiabatic case the hydrazines rotate in the opposite direction, and the hydrazine units rotate orthogonal to the bridge. This molecular motion switches the orbital overlap between the hydrazine units and the aromatic bridge off, thus keeping the overlap magnitude negligible at the crossing seam. Along the seam the Born−Oppenheimer approximation is not valid and the system can only pass efficiently from the reactant to the product well through vibrational and electronic coordinate mixing.

In conclusion, our results indicate that nonadabatic electron transfer and chemical electron transfer paths are distinct elements of the mechanistic spectrum of intramolecular electron transfer in radical cation systems. The nonadiabatic electron transfer process involves an unconventional reaction path with a "transition state" corresponding to a crossing seam (i.e., approximately an $(n-1)$-dimensional intersection, where $n$ is the number of vibrational degrees of freedom of the system). *To our knowledge this is the first documented example of a ground-state reaction coordinate that connects reactant and products via a nonavoided (i.e., real) crossing between two different adiabatic potential energy surfaces.*

**Acknowledgment.** All computations were carried out on an IBM-SP2 funded jointly by IBM-UK and HEFCE (UK). We are grateful to the European Community for a Marie Curie Fellowship to L.B. (Grant No. ERB4001GT964926). The colaboration between M.A.R. and M.O. is financed by Nato Grant CRG 950748.

**Supporting Information Available:** Cartesian coordinates of all structures reported (ASCII) and linearly interpolated reaction coordinate between the localized minimum **1** and **Quin1** (Figure S1). This material is available free of charge via the Internet at http://pubs.acs.org.

JA000013C